Biomaterials 232 (2020) 119725

Contents lists available at ScienceDirect

Biomaterials

journal homepage: www.elsevier.com/locate/biomaterials

Porous bio-click microgel scaffolds control hMSC interactions and promote their secretory properties

Alexander S. Caldwell[a,b,1], Varsha V. Rao[a,b,1], Alyxandra C. Golden[a], Kristi S. Anseth[a,b,*]

[a] Department of Chemical and Biological Engineering, University of Colorado, 3415 Colorado Avenue, Boulder, CO, 80303-0596, USA
[b] BioFrontiers Institute, University of Colorado, 3415 Colorado Avenue, Boulder, CO, 80303-0596, USA

ARTICLE INFO

Keywords:
Mesenchymal stem/stromal cell
Secretome
HAVDI peptide
Microgels
Porous scaffolds
Bio-click

ABSTRACT

Human mesenchymal stem/stromal cells (hMSCs) are known to secrete numerous cytokines that signal to endogenous cells and aid in tissue regeneration. However, the role that biomaterial scaffolds can play in controlling hMSC secretory properties has been less explored. Here, microgels were co-assembled with hMSCs using three different microgel populations, with large (190 ± 100 μm), medium (110 ± 60 μm), and small (13 ± 6 μm) diameters, to create distinct porous environments that influenced hMSC clustering. Cells embedded in large diameter microgel networks resided in large clusters (~40 cells), compared to small clusters (~6 cells) observed in networks using medium diameter microgels and primarily single cells in small diameter microgel networks. Using a cytokine microarray, an overall increase in secretion was observed in scaffolds that promoted hMSC clustering, with over 60% of the measured cytokines most elevated in the large diameter microgel networks. N-cadherin interactions were identified as partially mediating these differences, so the microgel formulations were modified with an N-cadherin epitope, HAVDI, to mimic cell-cell interactions. Results revealed increased secretory properties for hMSCs in HAVDI functionalized scaffolds, even the non-clustered cells in small diameter microgel networks. Together, these results demonstrate opportunities for microgel-based scaffold systems for hMSC delivery and tailoring of porous materials properties to promote their secretory potential.

1. Introduction

hMSCs are the one of the most commonly used adult stem cells in clinical trials [1]. Extensive research has documented the ability of hMSCs to differentiate into cells of a mesenchymal lineage (e.g., osteoblasts, chondrocytes, adipocytes) and to secrete numerous trophic factors. Specifically, hMSCs secrete a plethora of factors capable of influencing angiogenesis, fibrosis, apoptosis, cell differentiation, immune responses and cardiac, muscle, and neural tissue regeneration [3]. While much is known about the effects of biomaterial scaffold properties (matrix mechanics [4–7], dimensionality [8], porosity [9,10], adhesive ligand tethering [11,12], etc.) on hMSCs differentiation, the influence of these properties on the hMSC secretome is less known. As a result, there is a growing interest in understanding how scaffold delivery systems can be designed to influence their secretory properties and therapeutic outcomes [2,3].

Although cell-matrix interactions, including passage number and substrate mechanics [13,14], significantly affect the hMSC secretory phenotype, studies have documented the influence of cell-cell interactions in promoting increased secretion of cytokines [15]. For example, aggregating hMSCs in spheroid cultures increased survival and upregulated secretion of both VEGF and PGE2 compared to dissociated cells [16]. Spheroid size has also been implicated in directing hMSC secretory properties, with cells in larger spheroids (40,000 cells/spheroid) secreting elevated levels of several cytokines involved in inflammatory signaling, including GRO, IFN-γ, and IL-10 compared to cells in smaller spheroids (10,000 cells/spheroid) [17]. Further, Qazi et al. used porous alginate scaffolds to tailor the microenvironment to achieve higher levels of secreted cytokine in rat MSCs (rMSCs) [18]. rMSCs encapsulated in lyophilized alginate scaffolds with a mean pore size of 122 ± 29 μm secreted higher levels of cytokines and regenerative factors, specifically HGF, IGF, and FGF-2, compared to rMSCs encapsulated in bulk alginate hydrogels or plated on traditional plastic substrates. This work also implicated N-cadherin as a mediator for paracrine signaling in rMSCs; as blocking N-cadherin interactions decreased cytokine secretion in the scaffolds. Collectively, these studies support the notion that cell-cell connections, and particularly N-cadherin, is critical for enhanced paracrine signaling in MSCs. Based on this

* Corresponding author. Department of Chemical and Biological Engineering University of Colorado 3415 Colorado Avenue, Boulder, CO, 80303-0596, USA.
E-mail address: kristi.anseth@colorado.edu (K.S. Anseth).
[1] A.S. Caldwell and V.V. Rao contributed equally to this work.

https://doi.org/10.1016/j.biomaterials.2019.119725
Received 3 October 2019; Received in revised form 20 December 2019; Accepted 22 December 2019
Available online 27 December 2019
0142-9612/

premise, we designed 3D porous bio-click hydrogel scaffolds to manipulate and control hMSC cell-cell interactions in a systematic manner and then quantified the effect on the secretion of proteins using a cytokine array.

Caldwell et al. demonstrated a new method for assembling microgel scaffolds into porous cell laden scaffolds using azide-alkyne bioclick-reactions [19]. hMSCs were embedded in peptide functionalized poly (ethylene glycol) scaffolds with microgels of varying size to create distinct hMSC-material interactions and microenvironments. Changes in particle diameter lead to alterations in overall porosity, pore dimensions, and cell morphology. Building on this initial study, in this paper, microgels with a broader range of diameters and final pore dimensions were used to encapsulate hMSCs and control their cell-matrix versus cell-cell interactions. hMSC secretory properties are significantly altered with increased clustering resulting in higher secretion of several cytokines known to be important in hMSC based cell therapies. Immunostaining and quantitative image analysis suggested that N-cadherin interactions may be contributing to these differences. Thus, an N-cadherin mimicking peptide (HAVDI) was conjugated to the microgel formulations. Previously, HAVDI peptide has been conjugated to hyaluronan gels where it increased chondrogenic differentiation of hMSCs [20]. Here, experiments were designed to test whether HAVDI could mimic cell-cell interactions and promote the secretory properties of single or clustered cells encapsulated in microgel networks. Interestingly, principal component analysis showed that secretory properties were elevated for all HAVDI conditions and the secretory profiles of cells in different pore sizes were more similar to each other when HAVDI was included in the scaffolds. Overall, the results reported herein demonstrate the design of a porous bio-click hydrogel scaffolds that allow for hMSC encapsulation and manipulation of the secretory profile by controlling cell-cell interactions or incorporating bioactive moieties that promote cell-matrix interactions.

2. Materials and methods

2.1. Macromer synthesis and microgel polymerization

Eight-arm poly(ethylene glycol) (PEG) amine (JenKem, M_n~20,000 Da) was reacted with dibenzocylcooctyne (DBCO) as previously described [19]. End-group functionalization was confirmed by ^{1}H NMR to be > 85%. Four-arm PEG-azide (PEG-N_3) was also synthesized as previously described [21]. End-group functionalization was confirmed by ^{1}H NMR to be > 95%. A cellularly-adhesive peptide, GRGDS (RGD), and an N-cadherin mimicking peptide, GHAVDI (HAVDI), were synthesized using standard Fmoc chemistry and a Rink Amide MBHA resin (Chempep Inc, USA) on a Protein Technologies Tribute Peptide Synthesizer. An azide modified lysine analog (Fmoc-azide-L-lysine, ChemImpex) was used to synthesize an azide-labeled RGD (N_3-KGRGDS) and HAVDI (N_3-KGHAVDI). Peptides were purified using reverse phase High Pressure Liquid Chromatography (HPLC) and confirmed using Electrospray Ionization (ESI) mass spectroscopy.

Microgels were synthesized as previously described [19]. Briefly, microgels were fabricated using an inverse suspension polymerization in hexanes with Span-80 (2.25% v/v) and Tween-20 (0.75% v/v) using PEG-DBCO and PEG-N_3 macromers while an applied shear force was varied to control microgel size during polymerization. The applied shear was achieved using either magnetic stirring, vortexing, or sonication to create 190 ± 100 μm (large), 110 ± 60 μm (medium), and 13 ± 6 μm (small) microgels, respectively. Two distinct sets of microgels were prepared with 11 mM excess of either functional group to allow for subsequent scaffold assembly. N_3-GRGDS, was included in all microgels at a concentration of 1 mM, while N_3-HAVDI was included at the same 1 mM concentration for selected studies related to mimicking cell-cell interactions by modifying the microgel chemistry. Microgels were washed (under sterile conditions) with isopropanol (4x) and with phosphate buffered saline (PBS) (1x) before resuspension in PBS.

2.2. Characterization of porous microgel scaffolds

Microgel size and scaffold porosity were visualized by incorporating an azide labeled fluorophore (AlexaFluor 647 azide, Life Technologies, 0.04 mM) during microgel formation. Scaffold porosity was also visualized by swelling the networks with fluorescein isothiocyanate-dextran (Millipore Sigma, 2,000 kDa). The resulting porous scaffolds were then imaged on a laser scanning confocal (Zeiss LSM710) using a 10× water objective. The microgel diameter and pore size were quantified using previously published MATLAB codes [19]. Microgel storage moduli were assessed through shear rheology using a DH-R3 rheometer from TA Instruments, while scaffold mechanical properties were assessed through compressive rheology using an MTS Synergie 100.

2.3. hMSC isolation and culture

hMSCs were isolated from fresh bone marrow aspirate purchased from Lonza (donor 18-year-old black female). Following previously published protocols [13,22], hMSCs were isolated based on preferential adhesion to tissue culture polystyrene plates. Freshly isolated hMSCs were detached with 0.05% trypsin–EDTA (Sigma) and subsequently centrifuged, counted, and frozen in Cell Freezing Medium (Thermo Fisher). Only passage 2 or 3 cells were used for all encapsulation experiments. Growth media consisted of low glucose (1 ng/ml glucose) Dulbecco's Modified Eagle Medium (ThermoFisher) supplemented with 10% FBS (ThermoFisher), 1 ng/ml fibroblast growth factor basic (bFGF) (Life Technologies), 50 U/ml penicillin (ThermoFisher), 50 μg/ml streptomycin (ThermoFisher), 0.5 μg/ml of Amphotericin B (ThermoFisher). For secretion experiments, the same media was used sans bFGF (referred to as Experimental Media).

2.4. Cell encapsulation

Microgel scaffolds were fabricated by combining equal volumes (50 μL macromer volume) of DBCO-excess and N_3-excess microgels in 2 mL of PBS. The microgel suspensions were then centrifuged at 1000 rcf for 10 min, followed by 3000 rcf for 2 min. Microgel scaffolds were then placed in PBS and allowed to equilibrate in PBS, reaching a final swollen volume of ~200 μL in each case. To create cell-laden microgel scaffolds hMSCs (1 million cells) were mixed with microgels during network formation (cell density of 5 million cells/mL). After centrifugation scaffolds were immediately placed in experimental media.

2.5. Immunofluorescent staining

Three days after encapsulation, hMSCs in microgel networks were fixed by treatment with 10% formalin for 30 min at room temperature (RT). Samples were washed three times with PBS for 10 min at RT on shaker plate. Next, samples were permeabilized and blocked with 0.1% Triton X-100 and 5% bovine serum albumin (BSA) respectively in PBS for 1 hour at RT. Samples were incubated with anti-N-cadherin antibody (3 μg ml^{-1}, mouse, Invitrogen) in Cell Staining Buffer (Bio-rad) overnight at 4 °C. After three washes with PBST (0.5 wt% Tween-20 in PBS) for 10 min on the shaker, samples were incubated with goat anti-rabbit Alexaflour 488 (1:400, Invitrogen), DAPI (1:500, Sigma) and Rhodamine Phalloidin (1:300, Sigma Aldrich) for 1 h at RT in the dark. For cell cluster analysis, no primary antibody was added and only DAPI and Rhodamine Phalloidin was incubated for 1 hour at RT. Samples were imaged on either a Nikon Spinning Disc Confocal (40x air or 60× water objective) or a Zeiss Laser Scanning Confocal (20× air objective) microscopes.

2.6. Image analysis

Approximately 80 μm z-stack images (with < 1 μm intervals

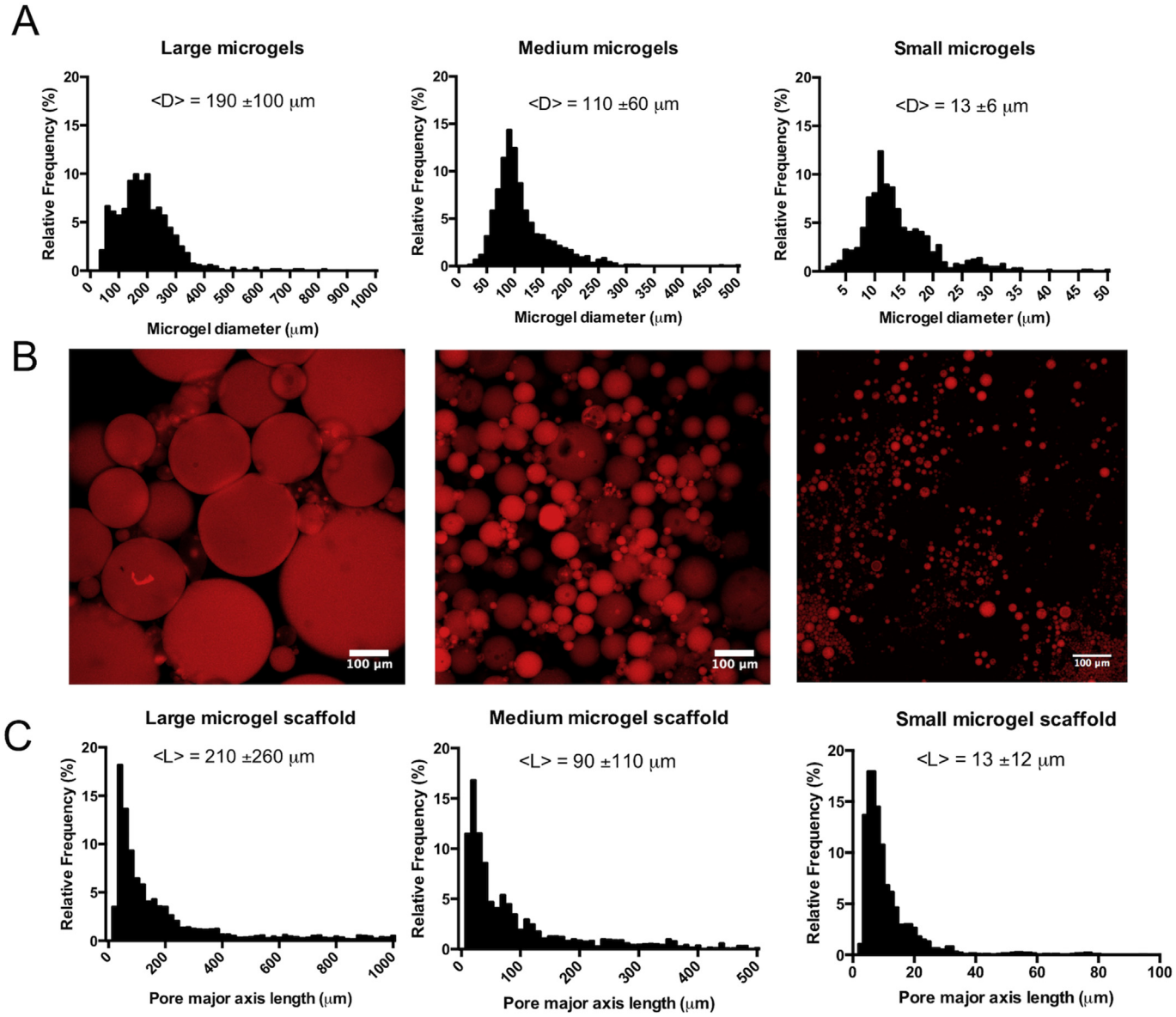

Fig. 1. Generation of varied porous scaffolds using clickable microgel building blocks. (A) Clickable microgel building blocks were synthesized using an inverse suspension polymerization out of 8-arm poly(ethylene glycol) (PEG) functionalized dibenzylcyclooctyne (DBCO), 4-arm PEG-N_3, and an azide functionalized cellularly adhesive peptide (GRGDS). During the polymerization shear was varied to create microgels with 190 ± 100 μm (left), 110 ± 60 μm (middle), and 13 ± 6 μm (right) mean particle diameters, termed large, medium, and small, respectively. (B) Microgel scaffolds were formed by co-assembling DBCO and N_3 particles for each size group (190 ± 100 μm (left), 110 ± 60 μm (middle), and 13 ± 6 μm (right)). Particles were visualized via incorporation of an azide labeled AlexaFluor 647 dye (C) The resulting microgel scaffold structures were categorized by measuring the pore mean major axes lengths. Pore lengths correlated with the microgel diameter, with average lengths of 210 ± 260 μm (large diameter, left), 90 ± 110 μm (medium diameter, middle), and 13 ± 12 μm (small diameter, right).

between slices) were imported into IMARIS 3D visualization software (Bitplane). For cell cluster analysis, a 3D surface was reconstructed using the F-actin stain in order to define the confines of a cell cluster. Next, nuclei were identified with Spots Analysis. Using a pre-written Matlab code (Split into Surface Objects Xtension) within the IMARIS software, the number of nuclei within each cluster was determined. A cluster was defined as possessing greater than 2 nuclei. The intensity of the N-cadherin punctate was performed using ImageJ. To start, maximum intensity projections of the images were compiled and duplicates converted to binary. Particles analysis was performed on the binary image and the intensities within particles were determined using the original maximum intensity projection. Outlier analysis was conducted using the ROUT method and Q = 1%. Over 150 punctate were analyzed for N = 3 gels per condition.

2.7. Secretome analysis

Global secretory profiles were measured using a Human Cytokine Array C5 (RayBiotech) and the manufacturer's protocol was followed. Briefly, media was collected from microgel samples after three days. Arrays were blocked and incubated with 1 mL of media from each condition and acellular controls for overnight at 4 °C. Each array was washed with manufacturer's washing buffer for three times. Next, the membranes were incubated with a biotinylated antibody cocktail for 2 hours at RT, washed, and then incubated with HRP-streptavidin for 2 hours at RT. After incubation of the detection buffers, chemiluminescence was detected using a charge-coupled device camera (ImageQuant LAS 4000 GE Health-care). Exposure and incubation times were kept constant between each condition and controls. Raw images

were analyzed using the 2D Array feature of ImageQuant (GE Healthcare). Background signal was subtracted, and average intensities were normalized to positive spot controls. Intensities from corresponding spots from control arrays were subtracted and each value was normalized to μg DNA as determined by Quant-it Pico Green assay.

Before running the assay, microgels scaffolds were homogenized with a TissueLyser II (Qiagen) at 30 Hz for 1 min and digested in with in 1 mg mL^{-1} Papain enzyme (Sigma) in PBE buffer containing 1.77 mg mL^{-1} L-cysteine overnight at 65 °C. DNA concentration per gel was determined using manufacturer's protocol for the Quant-it Pico Green assay.

ELISAs were performed according to the manufacturer's protocol for specific cytokine concentration quantification. VEGF and LIF ELISAs were purchased from R&D systems, GDNF from Thermo Fisher, IGF-1 from Ray Biotech. Concentration values were also normalized to μg DNA.

2.8. N-cadherin blocking

Blocking of N-cadherin cell-cell interactions was performed based on previously published protocols [18,23]. Briefly, trypsinized hMSCs were centrifuged, re-suspended in experimental media containing N-cadherin blocking antibody (50 μg/ml, Sigma-Aldrich GC4), and incubated for 45 min at 4 °C. The cells were then washed twice with PBS and encapsulated in microgels networks. 10 μg/mL of the N-cadherin blocking antibody was also included in the media throughout the experiments to ensure sustained blocking.

2.9. Statistical and principle component analysis

Statistical analysis of data for cell clustering (percentage of cells in a cluster and number of cells per cluster), and specific ELISAs were performed using GraphPad prism. Statistical significance was determined using one-way ANOVAs with Tukey post hoc comparisons. All conditions represent three independent biological replicates unless otherwise noted. Principle component analysis (PCA) was used to assess correlations between the secretory profiles of cells in each scaffold condition. All analysis and PCA plots were made using the software ClustVis.

3. Results

3.1. Generation of scaffolds with varying pore dimensions using clickable microgel units

Clickable PEG microgels with excess DBCO or N_3 functional groups were fabricated via an inverse suspension polymerization [19]. Three distinct populations of PEG microgels were synthesized with mean diameters of 190 ± 100 μm, 110 ± 60 μm, and 13 ± 6 μm (Fig. 1a). These populations will be subsequently referred to as large, medium, and small diameter microgels, respectively.

Microgel storage moduli were measured to be 12.3 ± 2.3 kPa and 2.1 ± 0.3 kPa for DBCO excess and N_3 excess particles, respectively (Supplementary Fig. S1a). Microgel scaffolds were assembled by mixing equal volumes of DBCO and N_3 microgel populations (large (190 ± 100 μm), medium (110 ± 60 μm), or small (13 ± 6 μm) diameters) and centrifuging to induce particle-particle interactions (Fig. 1b); the resulting porous microgel scaffolds were then characterized by light microscopy. Scaffold compressive moduli were measured to be 1.9 ± 0.3 kPa for large, 2.0 ± 0.4 kPa for medium, and 2.5 ± 0.2 kPa for small diameter microgel scaffolds, with no significant difference between conditions (Supplementary Fig. S1b). To improve visualization of the pore size within the microgel scaffolds, scaffolds were swollen with a high molecular weight fluorescent dextran (Supplementary Fig. S2). Each network condition maintained a similar three-dimensional structure, with interconnected pores of varying size throughout the microgel network. Pore structure, however, varied significantly between the conditions, with pore dimensions scaling with microgel size (Fig. 1c). The average pore diameter in large microgel networks was measured to be 210 ± 260 μm, 90 ± 110 μm in medium microgel networks, and 13 ± 12 μm in small microgel networks. The total porosity was similar for large and medium microgel scaffolds at 30.5 ± 0.2% and 28.8 ± 1.0%, respectively, while small microgel scaffolds were less porous with an overall void content of 10.9 ± 0.3% (Supplementary Table 1).

3.2. Human mesenchymal stem cell (hMSC) clustering scales with pore size

The size and frequency of clustered cells was determined using light microscopy and 3D visualization software (IMARIS). hMSCs were encapsulated in porous microgels networks fabricated with large (190 ± 100 μm), medium (110 ± 60 μm), and small (13 ± 6 μm) diameter microgels at a density of 5 million cells/mL. Centrifugation speeds and the encapsulation procedure have been previously optimized and reported as cytocompatible [19], and hMSCs in each condition were highly viable with no significant difference between conditions (96.3 ± 4.6% in large microgel scaffolds, 92.8 ± 4.0% in medium microgel scaffolds, and 94.2 ± 2.7% in small microgel scaffolds) (Supplementary Fig. S3). After three days in culture, samples were fixed, stained with DAPI and rhodamine phalloidin, and imaged on a Nikon spinning disc confocal microscope. Qualitative differences in the cell cluster size are readily observed between the three microgel conditions (Fig. 2a).

Z-stacks of the cell-laden microgel scaffolds were imported into IMARIS 3D visualization software and a 3D surface was rendered over a cluster by utilizing the cytoplasmic stain. The number of nuclei per cluster was determined using a Matlab code (Split into Surface Objects Xtension) in the IMARIS software. hMSC cluster size was analyzed for $N > 8$ gels for each particle size condition. An increase in pore size, a function of the microgel particle size, led to a higher percentage of cells residing in a cluster, defined as possessing three or more nuclei. This cluster threshold was chosen to assess cell-cell interactions during the microgel scaffold assembly and not as a result of cell division over 72 hours of culture time. In networks fabricated from large (190 ± 100 μm) diameter particles, almost all hMSCs resided within a cluster (98 ± 1.6%) (Fig. 2b). The percentage of cells in a cluster was significantly lower in both the medium (110 ± 60 μm) and small (13 ± 6 μm) diameter microgel networks, 68 ± 19% and 18 ± 21%, respectively. Each condition was statistically different than the others. Additionally, larger pore sizes caused an increase in the cluster size: ~40 ± 18 cells/cluster in the large microgel scaffolds, ~7 ± 3 cells/cluster in the medium and ~5 ± 1 cells/cluster in the small microgel networks. The average hMSC cluster size was not significantly different between the medium and small microgel scaffolds.

3.3. hMSC secretory properties vary with scaffold porosity and cluster size

After 72 hours in each culture condition (large (190 ± 100 μm), medium (110 ± 60 μm), or small (13 ± 6 μm) diameter microgel scaffolds), the secreted proteins in the media were measured using a cytokine array and normalized to DNA content to quantify the effect of scaffold properties on the hMSC cytokine secretion. A cytokine array was selected to quantify a broad number of cytokines and chemokines involved in hMSC paracrine signaling. Analyses revealed that the scaffold pore architecture strongly influenced the hMSC secretome (Fig. 3a). Cells encapsulated in the large microgel scaffolds demonstrated a distinct secretory profile, compared to relatively similar secretory profiles between the medium and small diameter microgel scaffolds. In general, hMSCs in the large diameter microgel scaffolds secreted higher concentrations (represented by red intensities on the heatmap) of cytokines compared to the lower concentrations (represented by blue intensities on the heatmap) by cells in the medium and small diameter microgel scaffolds. Of the 72 cytokines secreted at

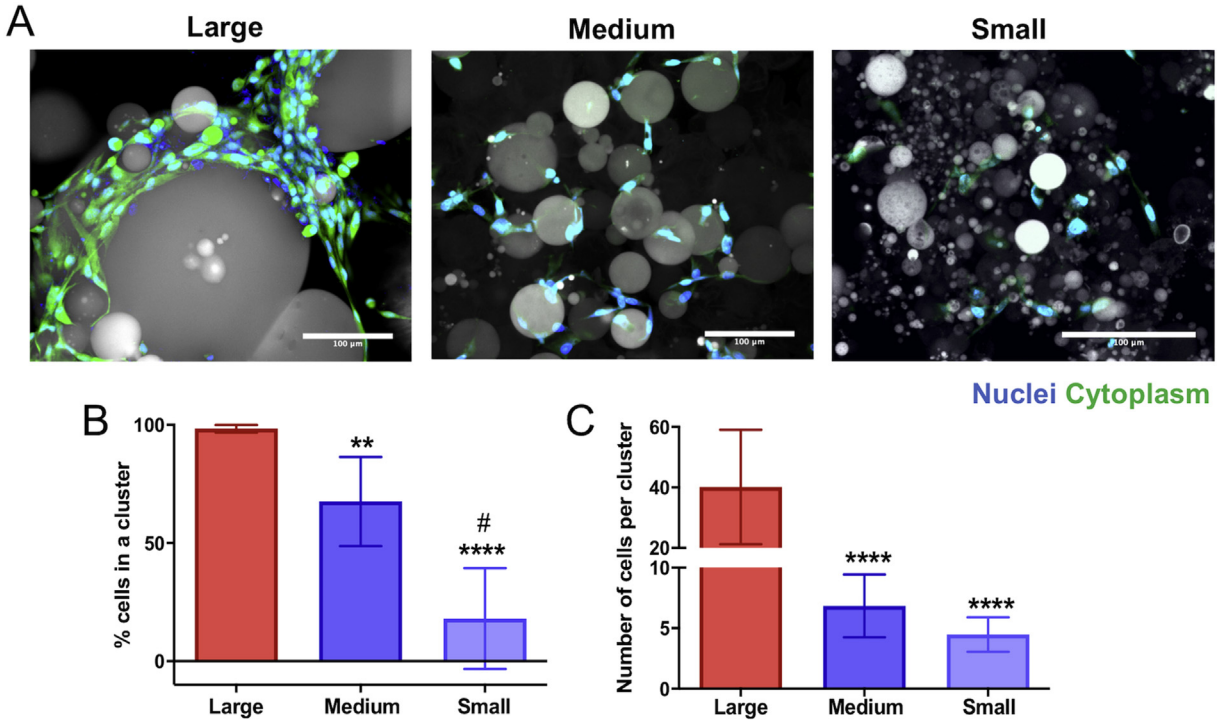

Fig. 2. Pore dimensions control human mesenchymal stem cell (hMSC) clustering in varied porous scaffolds. (A) Images of hMSCs cultured in large (190 ± 100 μm) diameter (left), medium (110 ± 60 μm) diameter (middle), and small (13 ± 6 μm) diameter (right) microgel scaffolds for 72 h. Cells stained for nuclei (blue, DAPI) and cytoplasm (green, Calcien) and particles shown via transmitted light. Scale bars = 100 μm. (B) Percent of cells in a cluster in each microgel condition. Cell-cell interactions were quantified by measuring the average number of cells in a cluster (3 or more cells physically touching) in each condition. (C) Average number of cells in a cluster was also quantified for each condition. Average number of cells per cluster between the medium and small microgel scaffolds was not significantly different. Significance determined using a one-way ANOVA. All stars represent significance compared to large microgel condition. ****$p < 0.0001$, **$p < 0.01$, #$p < 0.001$ (compared to medium diameter). (For interpretation of the references to colour in this figure legend, the reader is referred to the Web version of this article.)

detectable levels, 48 (~60%) were most elevated in the large diameter microgel scaffolds, while only 18 (25%) and 11 (~15%) were highest in the medium and small diameter microgel scaffolds, respectively (Fig. 3b). Beyond this global screen, a subset of factors was selected based on a literature review of hMSC regenerative therapies [24–27]. Of the 24 factors chosen, a similar trend was observed, with the majority of these regenerative cytokines (65%) being most elevated in networks formed from large microgels, compared to 21% in medium microgels, and 13% in small diameter microgel networks.

3.4. N-cadherin interactions increase with increased cell clustering

N-cadherins are a type I classical cadherin responsible for adherence junctions between cells primarily of the mesenchymal lineage. Cadherins are one of several membrane bound proteins that are involved in intercellular communication, with N-cadherins being the most widely expressed on hMSCs [28]. Since differential cell clustering occurred in the porous scaffold conditions, immunofluorescent staining was performed on encapsulated hMSCs to assess differences in cell-cell interactions mediated via N-cadherin. To adequately image and quantify the punctate, the microgels were not stained during imaging. In Fig. 4a (top), large N-cadherin punctae were observed in hMSC clusters in the large (190 ± 100 μm) diameter microgel scaffolds. In contrast, while hMSCs in the medium (110 ± 60 μm) diameter microgel scaffolds maintained some cell clustering and elevated N-cadherin staining (Fig. 4a, middle), the majority of hMSCs in the small (13 ± 6 μm) diameter microgel scaffolds did not reside in clusters and had more diffuse N-cadherin staining (Fig. 4a, bottom). These differences were further quantified by analysis of the N-cadherin punctate intensity and a significant increase in expression by hMSCs encapsulated in the large microgel scaffolds was observed (Fig. 4b).

3.5. Blocking N-cadherin interactions in microgel scaffolds decreases hMSC secretory properties

To further investigate the role of cell-cell interactions mediated via N-cadherin on the hMSC secretory phenotype, hMSCs were incubated with a monoclonal antibody against N-cadherin (αN-Cad) prior to encapsulation. The culture media was also supplemented with αN-Cad during the entire culture period. After 72 h, the cell media was collected and analyzed with a cytokine array as described above. Results revealed that blocking N-cadherin led to a significant decrease in the secretion of cytokines by hMSCs for all scaffold conditions (Fig. 5a). Notably, the expression of 78% of all measured cytokines was decreased in the large (190 ± 100 μm) diameter microgel scaffolds, while 44% and 46% of all cytokines were similarly decreased in the medium (110 ± 60 μm) and small (13 ± 6 μm) diameter microgel scaffolds, respectively. Over a ten-fold decrease was observed for 45% of cytokines in the large condition and 20% and 19% for the medium and small diameter microgel networks respectively. Only two factors in the large diameter microgel scaffold were upregulated by over ten-fold, while only 7 and 8 of factors were highly upregulated in medium and small diameter microgel scaffolds, respectively. Principal component analysis (PCA) was used to evaluate the differential role of N-cadherin interactions on the secretory profiles observed between the microgel networks. PC1 and PC2 explained 39.9% and 31.4% of the variance respectively. When examined this way, the secretory profile of hMSCs encapsulated in large diameter microgel scaffolds under standard culture conditions was distinct from those in medium and small diameter microgel networks (Fig. 5b). However, when the N-cadherin interactions were blocked, the secretory profile of the hMSCs in all pore conditions became similar. These results help quantify and illustrate the role that N-cadherin interactions and cell-cell clustering play in the dictating the secretory profiles of hMSCs.

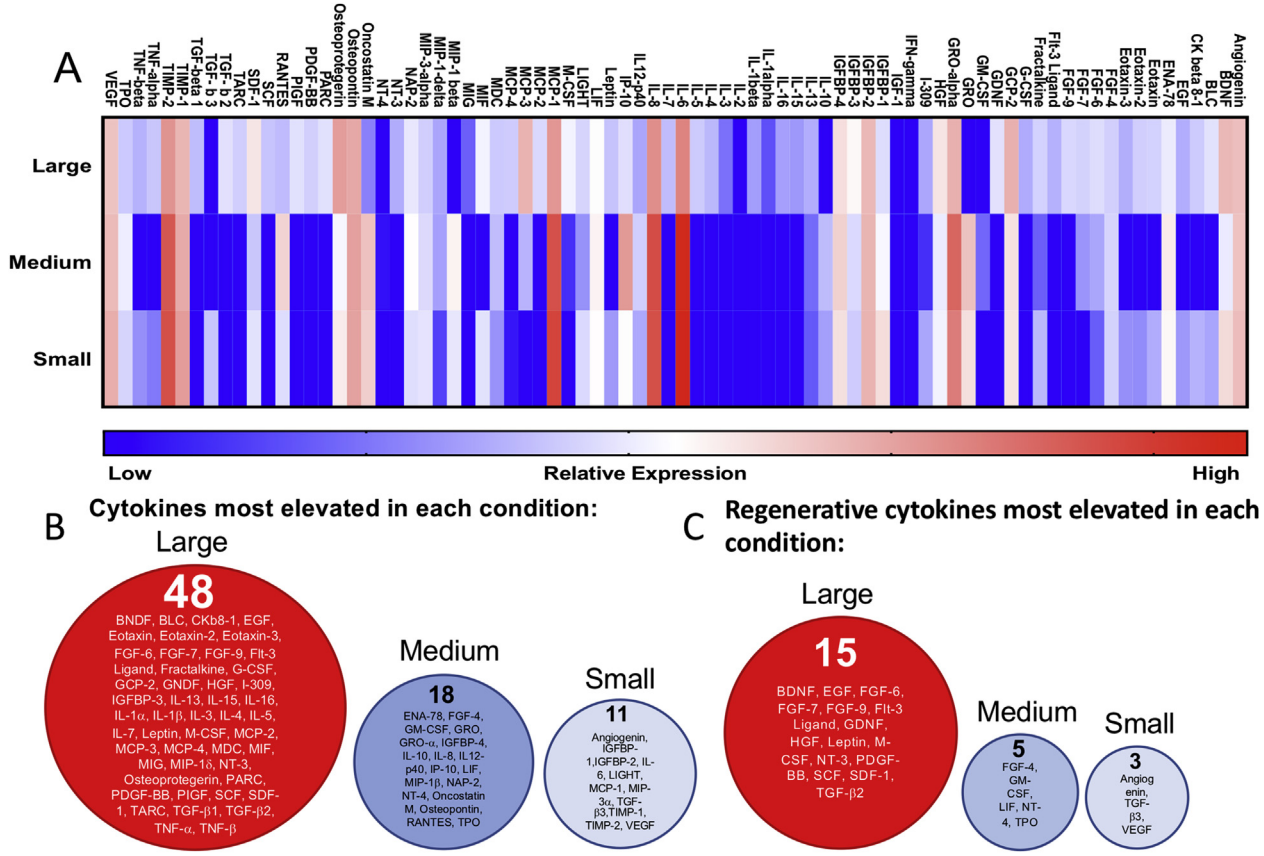

Fig. 3. hMSC secretory properties vary with scaffold porosity. (A) Heatmap of cytokine expression of encapsulated hMSCs in large (190 ± 100 μm), medium (110 ± 60 μm), and small (13 ± 6 μm) diameter microgel networks. Red intensities represent high expression while blue intensities represent low or undetectable expression levels compared to control (cell media). Values were normalized to DNA content. (B) Cytokines that were most elevated in large (left, red), medium (middle, blue), and small microgel scaffolds (right, light blue). (C) List of regenerative factors that were most elevated in large (left, red), medium (middle, blue), and small microgel scaffolds (right, light blue). (For interpretation of the references to colour in this figure legend, the reader is referred to the Web version of this article.)

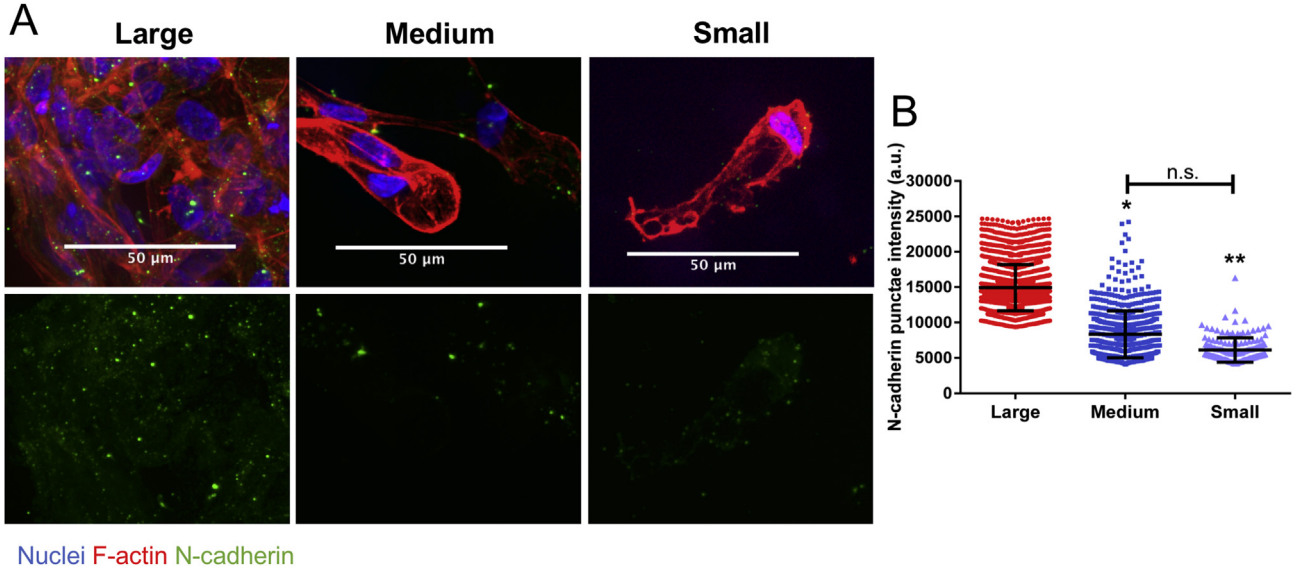

Fig. 4. N-cadherin interaction and expression increases with increased cell clustering. (A) hMSCs in large (190 ± 100 μm) diameter microgel scaffolds (top, right) with highly clustered cells show more intense staining for N-cadherin punctate compared with smaller clusters in medium (110 ± 60 μm) diameter microgel scaffolds (middle, right) and largely single cells in small (13 ± 6 μm) diameter microgel scaffolds (bottom, right) Cells stained for nuclei (blue), N-cadherin (green), and F-actin (red). (B) Intensity quantification of the N-cadherin punctate. Stars represent significance relative to large microgel scaffolds. **p < 0.01, *p < 0.05, n.s. – non-significant. (For interpretation of the references to colour in this figure legend, the reader is referred to the Web version of this article.)

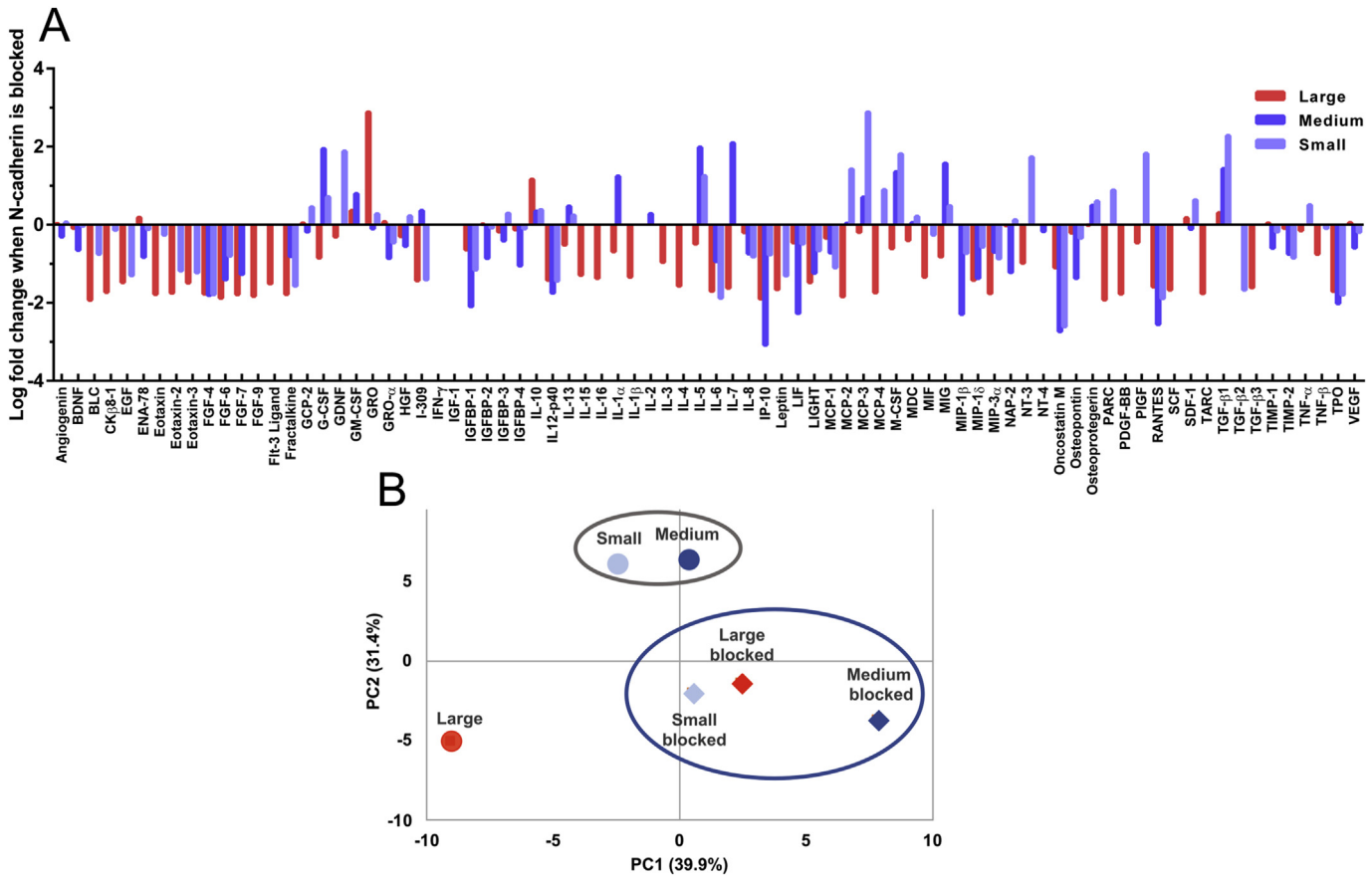

Fig. 5. Blocking N-cadherin interactions in microgel scaffolds decreases hMSC secretory properties. (A) Log-fold change in cytokine secretion from hMSCs in large (190 ± 100 μm) diameter (red), medium (110 ± 60 μm) diameter (blue), and small (13 ± 6 μm) diameter (light blue) microgel scaffolds when cultured in the presence of an anti-N-cadherin antibody compared to their respective unmodified conditions. Negative fold change indicates a decreased in cytokine expression in the presence of blocking. (B) Principal component analysis of hMSC secretory profile of standard conditions (circles) and N-cadherin blocked conditions (diamonds). Colors correspond to conditions in (A) PC1 and PC2 explained 39.9% and 31.4% of the variance, respectively. (For interpretation of the references to colour in this figure legend, the reader is referred to the Web version of this article.)

3.6. HAVDI functionalized microgel scaffolds promote the secretory phenotype of hMSCs

To engineer a microgel assembled scaffold to promote the secretory profile of hMSCs, even in the absence of cell-cell interactions, an N-cadherin mimetic peptide, HAVDI, was conjugated to the microgel formulations. hMSCs were cultured for 3 days in the same porous microgel system and the conditioned media was analyzed via cytokine arrays. The inclusion of the HAVDI peptide drastically increased the hMSC secretory profile in all scaffold conditions (Fig. 6a). Of all the eighty measured cytokines, 96% of them were increased in large (190 ± 100 μm) diameter microgel networks and 86% and 89% were increased in medium (110 ± 60 μm) and small (13 ± 6 μm) diameter microgel networks respectively (Fig. 6a). Of the previously identified regenerative cytokines (24), almost all (97%) were increased in large diameter microgel scaffolds, while 23 (96%) and 22 (92%) were elevated in the medium and small diameter microgel conditions respectively. Out of all the elevated cytokines, 33%, 42% and 45% were elevated 10-fold in large, medium, and small diameter microgel networks respectively. It should also be noted that no significant differences in hMSC cluster size or frequency of cells in clusters was observed due to the presence of the HAVDI (Supplementary Fig. S4). Thus, the primary effect was attributed to interactions between cells and HAVDI. Principal component analysis demonstrated that the secretory phenotype of hMSCs in HAVDI networks were more similar to each other compared to their unmodified counterparts (Fig. 6b). PC1 and PC2 explained 70.4% and 18.3% of the variance respectively.

Currently, the majority of hMSC clinical trials are focused on cardiovascular, neurological, inflammatory diseases, and bone/cartilage regeneration [1,29]. Cytokines secreted by hMSCs are integral to the success of many of these therapeutic applications [2,3]. Based on an analysis of hMSCs clinical trials focused on tissue regeneration, VEGF, GDNF, IGF-1, and LIF were selected for further analysis using ELISAs. Vascular endothelial growth factor (VEGF) is a key signaling cytokine involved in angiogenesis [30] and has been shown to improve MSC survival in infarct hearts where they can help repair cardiac tissue after myocardial infraction [31,32]. hMSCs secreted VEGF in all three pore size conditions (~1000–4000 pg/μg DNA) (Fig. 6a) but the HAVDI interactions increased secretion in medium and small diameter microgel scaffolds by 1.5-2-fold. A non-significant increase was observed in the large diameter microgel scaffolds (Fig. 6c). For neurodegenerative applications, glial cell-derived neurotrophic factor (GDNF) has restorative and protective effects on multiple neuronal cell types [33]. MSCs genetically modified to overexpressed GDNF provided local neuroprotection in an inflammatory model of Parkinson's [34]. GDNF was significantly elevated in each condition upon the addition of HAVDI (Fig. 6d). This was most noticeable in medium and small diameter microgel scaffolds, where GDNF levels rose by two orders of magnitude (~2 pg/μg DNA in unmodified conditions to > 250 pg/μg DNA in HAVDI conditions). IGF-1 is another anabolic cytokine that plays an important role in cardiac repair, as it can recruit and stimulate the differentiation of endogenous cells in the injured heart [35]. Low levels of IGF-1 secretion were observed in unmodified conditions (1–3 pg/μg DNA in large diameter microgel scaffolds, < 1 pg/μg DNA

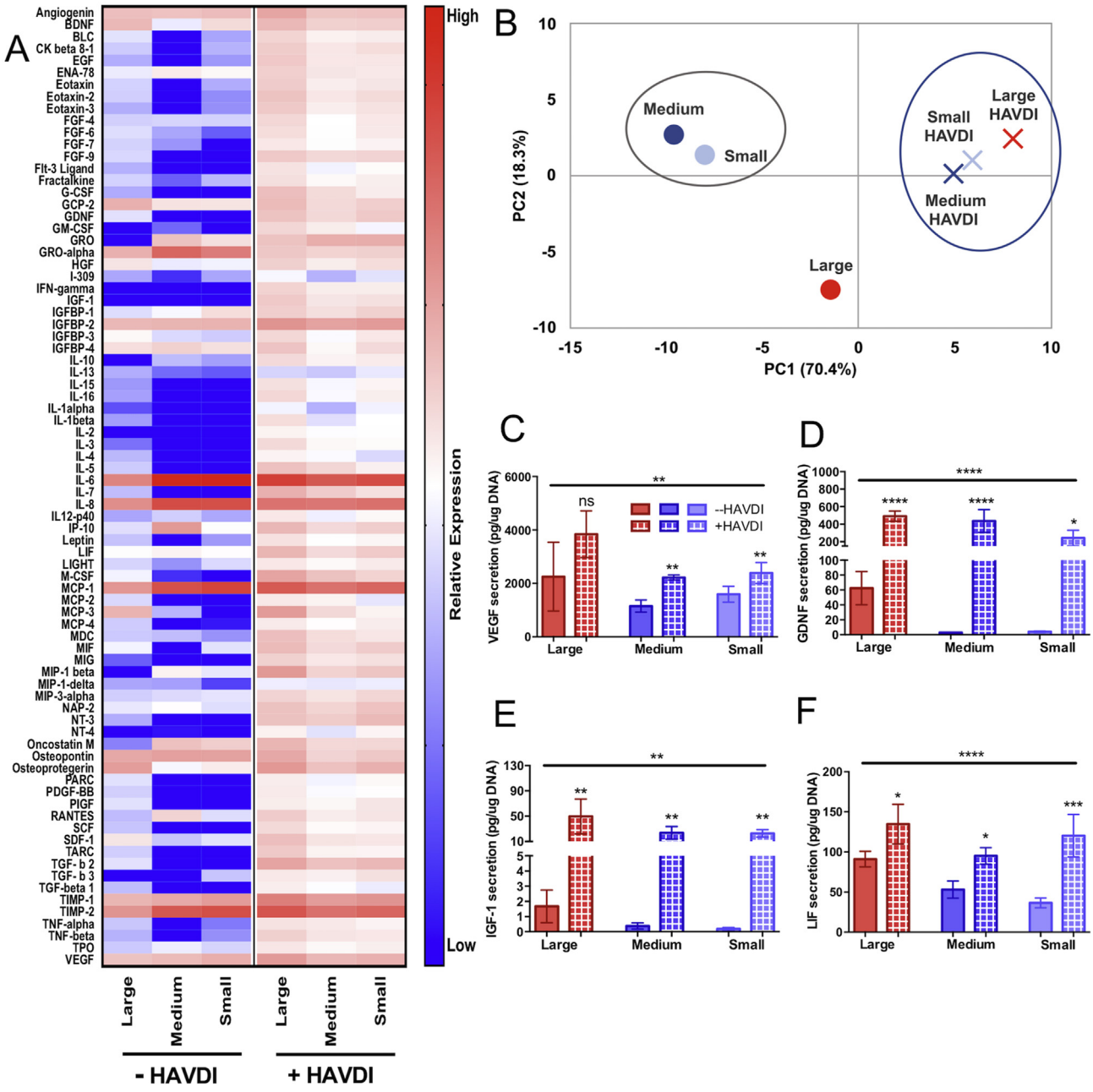

Fig. 6. – HAVDI inclusion in microgel scaffolds increases secretory phenotype of hMSCs. (A) Heatmap of cytokine expression of encapsulated hMSCs in large (190 ± 100 μm), medium (110 ± 60 μm), and small (13 ± 6 μm) diameter microgel scaffolds with and without inclusion of the HAVDI peptide. (B) PCA analysis of hMSC secretory profile between large (red), medium (blue), and small (light blue) microgel scaffolds without (circles) and with HAVDI (X symbol). PC1 and PC2 explained 70.4% and 18.3% of the variance respectively. (C) ELISA quantification of VEGF, (D) GDNF, and (E) IGF-1. HAVDI conditions are represented by hashed bars. Stars represent significance relative to respective unmodified scaffolds. Overall significance (top bar) determined using a one-way ANOVA with multiple comparisons. ****$p < 0.0001$, **$p < 0.01$, n.s. – non-significant. (For interpretation of the references to colour in this figure legend, the reader is referred to the Web version of this article.)

in medium and small diameter microgel scaffolds) but was elevated to 20–50 pg/μg DNA in HAVDI networks (Fig. 6e). Leukemia inhibitory factor (LIF) is involved in myogenic precursor cell recruitment and has also been implicated in myoblast proliferation and differentiation [36]. Significant upregulation in LIF secretion was observed in all scaffolds upon the addition of HAVDI, ranging from a 1.5-fold increase in large diameter microgel scaffolds to over a three-fold upregulation in small diameter microgel scaffold conditions (Fig. 6f). Combined, these data lend support to the notion that both the HAVDI peptide and cell clustering can promote the secretory properties of encapsulated hMSCs in microgel scaffolds.

4. Discussion

Porous scaffolds assembled from individual microgel components have drawn increased interest in the fields of biomaterials research and tissue regeneration. Several groups have demonstrated the versatile nature of this platform, where cross-linking reactions [37], incorporation of bioactive moieties [38,39], and particle size [40] can all be tuned to alter the final scaffold properties [41]. Often, a key design parameter is to create cell-instructive scaffolds, where microgels and cells are assembled together, and scaffold properties can be tuned to control multiple cell functions independently. Some examples include

directing matrix deposition [42], controlling cell motility [43], facilitating diffusion and nutrient transport [44], and mitigating immunogenic responses *in vivo* [41]. In this contribution, an assembled microgel scaffold was designed to control hMSC secretory properties via both physical and biochemical means. First, three particle sizes, 190 ± 100 μm, 110 ± 60 μm, and 13 ± 6 μm diameters, were used to created scaffolds with major axis pore lengths of ~210 μm, ~90 μm, and ~13 μm, respectively. Cells encapsulated in networks with 190 ± 100 μm (large) diameter particles were more frequently located in clusters (~98%) and the cluster sizes were larger (~40 cell/cluster) compared to less frequent (68% and 18%) and smaller clusters (7 and 5 cells/cluster) in 110 ± 60 μm (medium) and 13 ± 6 μm (small) diameter microgel scaffolds, respectively (Fig. 2). Increased cell-cell interactions significantly influenced hMSC secretory properties, where cells in large diameter microgel scaffolds secreted a higher level of a variety of proteins as assessed by a cytokine array. Approximately 60% of all cytokines measured were elevated in the large diameter microgel scaffolds. This data aligns with a growing body of literature demonstrating how scaffold porosity can affect cell function, such as dendritic cell activation [45,46] and hMSC osteogenic differentiation [47]. Of particular note, Qazi et al. demonstrated that pore size of gelatin scaffolds affected the angiogenic potential of hMSCs, with optimal secretion of angiogenic cytokines achieved in porous scaffolds that promoted clustering of infiltrating cells [48]. Together, these data demonstrate how pore size alone can be used to control cell-cell clustering and direct cell function.

In addition to manipulating pore size, several biochemical and physical strategies have been developed to improve the secretory properties of hMSCs, typically by exposing cells to exogenously delivered inflammatory molecules (i.e., licensing) [27,49] or by culturing hMSCs in large aggregates termed spheroids [15]. Additionally, it should be noted that MSCs be isolated from multiple tissues and cells can have varied secretory behavior based on their tissue of origin [50,51]. Murphy et al. used a hanging drop method to create hMSCs spheroids on the order of thousands of cell per aggregate and observed changes in secretion based on spheroid size [17]. In contrast, in the large microgel scaffolds presented in this study, there were ~1 million cells per gel and an average cluster size of 40 cells. Although it is difficult to compare spheroids directly with cells in porous scaffolds, the central theme of both is that hMSC cell-cell contacts contribute to their enhanced their secretory properties.

hMSCs are known to interact with each other via N-cadherins, which contain an extracellular domain that dimerizes between bound cells and an intracellular domain anchored to the cytoskeleton capable of signal transduction through several catenin mediated pathways [28]. In our centrifugation approach for the scaffold assembly, hMSCs had high levels of N-cadherin expression in the large clusters present in large (190 ± 100 μm) diameter microgel scaffolds (Fig. 4), and decreased expression in the small cell clusters present in the 110 ± 60 μm (medium) and 13 ± 6 μm (small) diameter microgel scaffolds. The role of the N-cadherin interactions on the hMSC secretory phenotype was further confirmed by blocking the interactions with a monoclonal antibody against N-cadherin. A marked decrease in secretion of a variety of different cytokines was observed in all conditions, but most noticeably in the large diameter microgel scaffolds, secretion was decreased ~78% for all of the measured cytokines (Fig. 5a). Further implicating the role of N-cadherin in influencing the hMSC secretory phenotype, the profile of hMSCs between conditions was more similar when N-cadherin was blocked compared to standard culture, as determined by principal component analysis (Fig. 5b). These data align with previous investigations, where the inclusion of a N-cadherin blocking antibody in porous and bulk hydrogels decreased the hMSC secretory phenotype, as assessed via a cytokine array [18].

To test whether cell-matrix interactions could mimic some of the same benefits as cell-cell interactions, an N-cadherin peptide epitope (HAVDI) was introduced into the microgel formulation to promote a secretory phenotype. While its role in hMSC differentiation and mechanosensing has previously been studied [20,23], less is known of its ability to stimulate hMSC secretory properties. The inclusion of HAVDI did not significantly alter hMSC multipotency, as assessed by CD105 expression (Supplementary Fig. S4a). However, it boosted cytokine secretion in all pore sizes, including VEGF, GDNF, LIF, and IGF-1 (Fig. 6) without altering cell cluster characteristics (Supplementary Fig. S4b,c). Additionally, PCA analysis confirmed that the secretory phenotype of cells in HAVDI scaffolds were more similar to each other than when in unmodified conditions. This approach may prove advantageous for design of biomaterial delivery systems for cell transplantation, where cell clustering is prohibited or non-ideal, but a secretory phenotype is beneficial for therapeutic outcomes. Design of scaffolds that can promote not only the survival, but secretion profiles of delivered cells may provide specific benefits for cell-based therapies for regenerative medicine.

5. Conclusions

The therapeutic potential of hMSCs paracrine factors is quickly being recognized; necessitating the development of biomaterial systems to deliver and promote secretory hMSCs. In this study, porous bio-click microgel assembled scaffolds were designed to control the secretory phenotype of hMSCs. First, microgel scaffold pore size was used to control hMSC aggregate size, allowing for increased secretory properties with highly clustered cells. Secondly, an N-cadherin mimetic peptide (HAVDI) was included to enhance hMSC cytokine secretion, in both clustered and singly encapsulated cell conditions. The ability to improve cell secretory behavior even when it is limited by other factors (i.e. lack of cell clustering) holds promise for improving cell-based therapies. These findings are relevant for informing biomaterial design both in *in vitro* studies as well the delivery of hMSCs for clinical applications.

Data sharing

The raw data used in this study are available from the corresponding author upon reasonable request.

Acknowledgments

This work was supported by the National Institutes of Health, United States (Grant: R01 DE016523). Alyxandra Golden was supported in part by a grant to the Biological Sciences Initiative at the University of Colorado Boulder, United States from the Howard Hughes Medical Institute's Undergraduate Science Education Program.

Appendix A. Supplementary data

Supplementary data to this article can be found online at https://doi.org/10.1016/j.biomaterials.2019.119725.

References

[1] A. Trounson, C. Mcdonald, Cell stem cell stem cell therapies in clinical trials: progress and challenges, Stem Cells (Dayton) 17 (2015) 11–22.
[2] A.I. Caplan, D. Correa, The MSC: an injury drugstore, Cell Stem Cell 9 (2011) 11–15.
[3] L. da Silva Meirelles, A.M. Fontes, D.T. Covas, A.I. Caplan, Mechanisms involved in the therapeutic properties of mesenchymal stem cells, Cytokine Growth Factor Rev. 20 (2009) 419–427.
[4] N. Huebsch, et al., Matrix elasticity of void-forming hydrogels controls transplanted-stem-cell-mediated bone formation, Nat. Mater. 14 (2015) 1269–1277.
[5] A.J. Engler, S. Sen, H.L. Sweeney, D.E. Discher, Matrix elasticity directs stem cell lineage specification, Cell 126 (2006) 677–689.
[6] W.L. Murphy, T.C. McDevitt, A.J. Engler, Materials as stem cell regulators, Nat. Mater. 13 (2014) 547–556.
[7] A.R. Killaars, et al., Extended exposure to stiff microenvironments leads to persistent chromatin remodeling in human mesenchymal stem cells, Adv. Sci. 6 (2019)

1801483.
[8] S.R. Caliari, S.L. an Vega, M. Kwon, E.M. Soulas, J.A. Burdick, Dimensionality and spreading influence MSC YAP/TAZ signaling in hydrogel environments, Biomaterials 103 (2016) 314–323.
[9] A. Di Luca, et al., Influencing chondrogenic differentiation of human mesenchymal stromal cells in scaffolds displaying a structural gradient in pore size, Acta Biomater. 36 (2016) 210–219.
[10] M.J. Gupte, et al., Pore size directs bone marrow stromal cell fate and tissue regeneration in nanofibrous macroporous scaffolds by mediating vascularization, Acta Biomater. 82 (2018) 1–11.
[11] F. Karimi, A.J. O'Connor, G.G. Qiao, D.E. Heath, Integrin clustering matters: a review of biomaterials functionalized with multivalent integrin-binding ligands to improve cell adhesion, migration, differentiation, angiogenesis, and biomedical device integration, Adv. Healthc. Mater. 1–28 (2018) 1701324.
[12] J.A. Burdick, K.S. Anseth, Photoencapsulation of osteoblasts in injectable RGD-modified PEG hydrogels for bone tissue engineering, Biomaterials 23 (2002) 4315–4323.
[13] V.V. Rao, M.K. Vu, H. Ma, A.R. Killaars, K.S. Anseth, Rescuing mesenchymal stem cell regenerative properties on hydrogel substrates post serial expansion, Bioeng. Transl. Med. 4 (2019) 51–60.
[14] A.A. Abdeen, J.B. Weiss, J. Lee, K.A. Kilian, Matrix composition and mechanics direct proangiogenic signaling from mesenchymal stem cells, Tissue Eng. A (2014) 1–9 00.
[15] M.A. Gionet-Gonzales, J.K. Leach, Engineering principles for guiding spheroid function in the regeneration of bone, cartilage, and skin, Biomed. Mater. 13 (2018) 034109.
[16] S.S. Ho, K.C. Murphy, B.Y.K. Binder, C.B. Vissers, J.K. Leach, Increased survival and function of mesenchymal stem cell spheroids entrapped in instructive alginate hydrogels, Stem Cells Transl. Med. 5 (2016) 773–781.
[17] K.C. Murphy, et al., Multifactorial experimental design to optimize the anti-inflammatory and proangiogenic potential of mesenchymal stem cell spheroids, Stem Cells 35 (2017) 1493–1504.
[18] T.H. Qazi, D.J. Mooney, G.N. Duda, S. Geissler, Biomaterials that promote cell-cell interactions enhance the paracrine function of MSCs, Biomaterials 140 (2017) 103–114.
[19] A.S. Caldwell, G.T. Campbell, K.M.T. Shekiro, K.S. Anseth, Clickable microgel scaffolds as platforms for 3D cell encapsulation, Adv. Healthc. Mater. 6 (2017) 1–8.
[20] L. Bian, M. Guvendiren, R.L. Mauck, J.A. Burdick, Hydrogels that mimic developmentally relevant matrix and N-cadherin interactions enhance MSC chondrogenesis, 110 (2013) 10117–10122.
[21] C.A. Deforest, B.D. Polizzotti, K.S. Anseth, Sequential click reactions for synthesizing and patterning three-dimensional cell microenvironments, Nat. Mater. (2009), https://doi.org/10.1038/nmat2473.
[22] C. Yang, M.W. Tibbitt, L. Basta, K.S. Anseth, Mechanical memory and dosing influence stem cell fate, Nat. Mater. 113 (2014) 645–651.
[23] B.D. Cosgrove, et al., N-cadherin adhesive interactions modulate matrix mechanosensing and fate commitment of mesenchymal stem cells, Nat. Mater. 15 (2016) 1297–1306.
[24] U. Galderisi, A. Giordano, The gap between the physiological and therapeutic roles of mesenchymal stem cells, Med. Res. Rev. 34 (2014) 1100–1126.
[25] S.H. Ranganath, O. Levy, M.S. Inamdar, J.M. Karp, Harnessing the mesenchymal stem cell secretome for the treatment of cardiovascular disease, Cell Stem Cell 10 (2012) 244–258.
[26] Q. Lian, X. Liang, Y. Ding, Y. Zhang, H.-F. Tse, Paracrine mechanisms of mesenchymal stem cell-based therapy: current status and perspectives, Cell Transplant. 23 (2014) 1045–1059.
[27] J.R. Ferreira, et al., Mesenchymal stromal cell secretome: influencing therapeutic potential by cellular pre-conditioning, Front. Immunol. 9 (2018) 2837.
[28] B.M. Gumbiner, Regulation of cadherin-mediated adhesion in morphogenesis, Nat. Rev. Mol. Cell Biol. 6 (2005) 622–634.
[29] U. Galderisi, T. Squillaro, G. Peluso, Clinical trials with mesenchymal stem cells: an update, Cell Transplant. 25 (2016) 829–848.
[30] N. Ferrara, H.P. Gerber, J. LeCouter, The biology of VEGF and its receptors, Nat. Med. 9 (2003) 669–676.
[31] J. Pons, et al., VEGF improves survival of mesenchymal stem cells in infarcted hearts, Biochem. Biophys. Res. Commun. 376 (2008) 419–422.
[32] J.M. Tang, et al., VEGF/SDF-1 promotes cardiac stem cell mobilization and myocardial repair in the infarcted heart, Cardiovasc. Res. 91 (2011) 402–411.
[33] C.F. Ibáñez, J.-O. Andressoo, Biology of GDNF and its receptors — relevance for disorders of the central nervous system, Neurobiol. Dis. 97 (2017) 80–89.
[34] D.B. Hoban, L. Howard, E. Dowd, GDNF-secreting mesenchymal stem cells provide localized neuroprotection in an inflammation-driven rat model of Parkinson's disease, Neuroscience 303 (2015) 402–411.
[35] H.K. Haider, S. Jiang, N.M. Idris, M. Ashraf, Cellular Biology IGF-1-Overexpressing Mesenchymal Stem Cells Accelerate Bone Marrow Stem Cell Mobilization via Paracrine Activation of SDF-1/CXCR4 Signaling to Promote Myocardial Repair, (2008), https://doi.org/10.1161/CIRCRESAHA.108.186742.
[36] L.C. Hunt, J. White, The role of leukemia inhibitory factor receptor signaling in skeletal muscle growth, injury and disease, in: J. White, G. Smythe (Eds.), Growth Factors and Cytokines in Skeletal Muscle Development, Growth, Regeneration and Disease, vols. 45–59, Springer International Publishing, 2016, , https://doi.org/10.1007/978-3-319-27511-6_3.
[37] E. Sideris, et al., Particle hydrogels based on hyaluronic acid building blocks, ACS Biomater. Sci. Eng. 2 (2016) 2034–2041.
[38] E.A. Scott, M.D. Nichols, R. Kuntz-Willits, D.L. Elbert, Modular scaffolds assembled around living cells using poly(ethylene glycol) microspheres with macroporation via a non-cytotoxic porogen, Acta Biomater. 6 (2010) 29–38.
[39] J.L. Roam, et al., A modular, plasmin-sensitive, clickable poly(ethylene glycol)-heparin-laminin microsphere system for establishing growth factor gradients in nerve guidance conduits, Biomaterials 72 (2015) 112–124.
[40] N.F. Truong, et al., Microporous annealed particle hydrogel stiffness, void space size, and adhesion properties impact cell proliferation, cell spreading, and gene transfer, Acta Biomater. 94 (2019) 160–172.
[41] D.R. Griffin, W.M. Weaver, P.O. Scumpia, D. Di Carlo, T. Segura, Accelerated wound healing by injectable microporous gel scaffolds assembled from annealed building blocks, Nat. Mater. (2015), https://doi.org/10.1038/nmat4294.
[42] G. Imparato, F. Urciuolo, C. Casale, P.A. Netti, The role of microscaffold properties in controlling the collagen assembly in 3D dermis equivalent using modular tissue engineering, Biomaterials 34 (2013) 7851–7861.
[43] J. Koh, et al., Enhanced in vivo delivery of stem cells using microporous annealed particle scaffolds, Small (2019) 1903147, https://doi.org/10.1002/smll.201903147.
[44] M.-H. Yao, et al., Directed self-assembly of polypeptide-engineered physical microgels for building porous cell-laden hydrogels, Chem. Commun. 50 (2014) 9405–9408.
[45] J. Kim, W.A. Li, W. Sands, D.J. Mooney, Effect of pore structure of macroporous poly(lactide-co-glycolide) scaffolds on the in vivo enrichment of dendritic cells, ACS Appl. Mater. Interfaces 6 (2014) 8505–8512.
[46] R. Chen, H. Ma, L. Zhang, J.D. Bryers, Precision-porous templated scaffolds of varying pore size drive dendritic cell activation, Biotechnol. Bioeng. 115 (2018) 1086–1095.
[47] C.A.B. Vissers, J.N. Harvestine, J.K. Leach, Pore size regulates mesenchymal stem cell response to Bioglass-loaded composite scaffolds, J. Mater. Chem. B 3 (2015) 8650–8658.
[48] T.H. Qazi, et al., Extrusion Printed Sca Ff Olds with Varying Pore Size as Modulators of MSC Angiogenic Paracrine E Ff Ects, (2019), https://doi.org/10.1021/acsbiomaterials.9b00843.
[49] Mao, A. S. et al. Programmable microencapsulation for enhanced mesenchymal stem cell persistence and immunomodulation. doi:10.1073/pnas.1819415116.
[50] R. Hass, C. Kasper, S. Böhm, R. Jacobs, Different populations and sources of human mesenchymal stem cells (MSC): a comparison of adult and neonatal tissue-derived MSC, Cell Commun. Signal. 9 (2011).
[51] A.O. Pires, et al., Unveiling the differences of secretome of human bone marrow mesenchymal stem cells, adipose tissue-derived stem cells, and human umbilical cord perivascular cells: a proteomic analysis, Stem Cells Dev. 25 (2016) 1073–1083.